Circumpolar ocean stability on Mars 3 Gy ago

Frédéric Schmidt, Michael J. Way, François Costard, Sylvain Bouley, Antoine Séjourné, Igor Aleinov

Circumpolar ocean stability on Mars 3 Gy ago

Frédéric Schmidt, Michael J. Way, François Costard, Sylvain Bouley, Antoine Séjourné, Igor Aleinov

Circumpolar Ocean stability on Mars 3 Gy ago

Schmidt Frédéric[a,b,1,2], **Way Michael J.**[c,d,e,1], **Costard François**[a], **Bouley Sylvain**[a,b,f], **Séjourné Antoine**[a], **and Aleinov Igor**[c,g]

[a]Université Paris-Saclay, CNRS, GEOPS, 91405, ORSAY, FRANCE; [b]Institut Universitaire de France (IUF); [c]NASA/Goddard Institute for Space Studies, 2880 Broadway, NY, NY 10025, USA; [d]GSFC Sellers Exoplanet Environments Collaboration, Greenbelt, MD, USA; [e]Theoretical Astrophysics, Department of Physics and Astronomy, Uppsala University, Uppsala, SWEDEN; [f]IMCCE – Observatoire de Paris, CNRS-UMR 8028, Paris, France; [g]Center for Climate Systems Research, Columbia University, New York, NY 10025, USA

This manuscript was compiled on September 24, 2021

What was the nature of the Late Hesperian climate? Warm and wet or cold and dry? Formulated this way the question leads to an apparent paradox since both options seem implausible. A warm and wet climate would have produced extensive fluvial erosion but few valley networks have been observed at the age of late Hesperian. A cold and dry climate would have kept any northern ocean frozen most of the time. But this would prevent tsunami formation, for which there is some evidence. Here, we provide new insights from numerical climate simulations in agreement with surface geological features to demonstrate that the Martian climate could have been both cold and wet. Using an advanced General Circulation Model (GCM), we demonstrate that an ocean can be stable, even if the Martian mean surface temperature is lower than 0°C. Rainfall is moderate near the shorelines and in the ocean. The southern plateau is mostly covered by ice with a mean temperature below 0°C. This climate is achieved with a 1 bar CO_2 dominated atmosphere with 10% H_2. Under this scenario 3 Ga, the geologic evidence of a shoreline and tsunami deposits along the ocean/land dichotomy are compatible with ice sheets and glacial valleys in the southern highlands.

Mars | Paleoclimate | Dynamic ocean | Ice sheet

The possibility of a late Martian ocean is a topic of debate with strong implications on the habitability of the Red Planet (1). A review of this controversy has been proposed recently (2). There is evidence of Martian paleo-shorelines (3) in Deuteronilus Mensae (sometimes noted contact No 2) in a geometry close to the current equipotential height (4). The Deuteronilus shoreline seems to be formed during the last stage of the true polar wander induced by Tharsis (5). A northern ocean is also supported by specific radar properties (6), smooth surface roughness (7) and by a fractal analysis of the topography (8). Crater counting datation of the Vastitas Borealis Formation near Deuteronilus Mensae is 3.5 Ga (9) but the ocean can be more recent. Detailed studies in Kasei Valles imply that such an ocean rose in elevation ($\sim$ 1000 m) between ca. 3.6 Ga and 3.2 Ga (10). Along this shoreline, tsunami deposits have been identified at an age of 3 Ga (11, 12) with at least two impact events. The Lomonosov crater morphology is coherent with an impact in shallow water, at the very same age of the tsunami deposits (13) and is thus the most probable source.

The stability of an ocean in a warm and wet scenario, even transient, at 3 Ga has been questioned since intense and widespread rainfall in such a scenario is not consistent with few observed dendritic valley networks from this time (14, 15). In previous work, a cold and wet Mars seemed impossible since the long term stability of an ocean (open or ice covered) in such a scenario has never been achieved by a 3D-GCM (14–19). Nevertheless, liquid brines are possible in this case but only with significant anti-freezing properties (20).

Cool and wet scenarios in the case of a faint young sun (in the Noachian-Hesperian boundary at 3.6 Ga) demonstrated that the ocean freezes for pressure below 1 bar and still predict intense rainfall when average temperature is higher than 0°C (21). An investigation with 2D simulations for early Mars argues for warm and semi-arid early Mars (22) but stresses the need for a coupled ocean/atmosphere model.

3D climate model

We present fully coupled ocean/atmosphere 3-D General Circulation Model simulations based on ROCKE-3D (23, hereafter R3D), which is based upon a parent Earth Climate Model known as ModelE2 (24). R3D allows us to estimate the interaction between atmosphere/ocean circulation but also encompasses a surface hydrological scheme. We assume the solar luminosity to be $\sim$ 79% (25) of its current value (1360.67 $W.m^{-2}$), hence at 3 Ga, the flux at Mars was set to 452.8 $W.m^{-2}$. The total water budget is 150 m GEL to fill the ocean basin in the north and Hellas. The ocean model has 13 layers to a hypothetical depth of 4647m. The ocean bathymetry is determined by the topography. In Hellas basin the ocean depth reaches 3194m (level 12 of 13) while in the northern ocean it is 1294m (level 10 of 13). A detailed description of the ocean is documented in (23). The sea ice is interactive and is determined by the salinity and corresponding freezing point of water and is again documented in (23). The salinity was set to modern Earth ocean values given the lack of constraints for ancient Mars, but R3D is capable of a range of salinities (26). In addition, the glacier mass must be added but the thickness of glacier cannot be constraint by our model. In any case, the water budget must be compatible with D/H measurements that implies 100-300 m GEL in the Hesperian (27, 28).

Four sets of numerical simulations were performed for 0°, 20°, 40°, 60° obliquity, with 1 bar atmospheric pressure (15, 29). For 20% H_2 in a CO_2 dominated atmosphere the

Significance Statement

The current Martian climate is not habitable and far from Earth's climate. At the same time that Life spread on Earth (3 Gy ago), the Red Planet was possibly more similar to our Blue Planet. Our model includes a coupled model with dynamic ocean and atmosphere including a hydrological cycle. We show that an ocean is stable in agreement with some geological records.

Please provide details of author contributions here.

Please declare any competing interests here.

[1]F.S. contributed equally to this work with M.J.W.

[2]To whom correspondence should be addressed. E-mail: frederic.schmidt@@universite-paris-saclay.fr

greenhouse effect is efficient enough to warm the entire planet, as expected (21). The average surface temperature is always greater than 10°C with a stable ocean (Northern ocean and Hellas basin sea) and intense rainfall, corresponding to the warm and wet scenario (30). For 10% H_2 the globally averaged surface temperature is below 0°C but the Northern ocean surface temperature remains surprisingly around 6°C and is thus stable from freezing. The source of H_2 may be volcanic or serpentinization, but such large concentration is not expected for more than My (31–33). The lower limit of H_2 necessary to stabilize the ocean will be matter of a future investigation.

Figure 1 shows the simulated surface fields averaged over 10 Martian years for H_2=10% and obliquity 40°. Interestingly this climate changes only slightly with obliquity (See Sup. Mat.). The major effect of water, ice and snow dependence on incidence angles are included (See Materials and Methods). The relatively modest effect of obliquity is due to the 1 bar atmospheric engine that redistribute more efficiently the heat than at present-day 6 mbar.

Despite an average temperature below 0°C, the ocean remains above freezing due to its circulation, low altitude and low albedo. The effect of circulation is a regional warming in the Northern region of 2.5°C (see Sup Mat. Figure 10). Figure 2 top shows the horizontal heat flux contributing to the ocean stabilization. Streamlines show the effect of ocean gyres transporting heat poleward, as expected for fast-rotating planet (34). Figure 2 bottom presents the surface temperature increase due to the active circulation of the ocean, as a function of latitude. At 0° obliquity, the increase is 0.5°C in average on the full planet but up to 2.5°C in the Northern polar ocean region. At 40° obliquity, the increase is 2.0°C in average but up to 2.5°C in the Northern region.

On land, there is a clear boundary at the 0°C isotherm which corresponds approximately to the Martian dichotomy. The altitude of the boundary varies from -700 to -3000 meters for obliquity from 0° to 60°.

In the high altitude domain, commonly referred to as the "icy highlands", the surface is mostly frozen and snow precipitation is dominant. The extensive accumulation of snow in the highlands can lead to the formation of significant ice sheets that may flow down to the Northern ocean and Hellas basin ocean. Our current model is not able to simulate details regarding the glacier flow, but only a global mass flux from land to the ocean. Glacial processes such as accumulation (snow compaction), flow (path, erosion), and ablation (direct melting, fluvio-glacial river) are thus not included. Nevertheless, the global mass flux (see Materials and Methods) is estimated around 3×10^{15} kg.y^{-1} and seems to be very robust to obliquity changes and H_2 content. For comparison, this flux is currently 1 to 5×10^{14} kg.y^{-1} on the Earth (35). Given the relative sizes of the planetary bodies, our value is relatively high.

In the lowest altitude domain, called the "wet lowlands", rain, evaporation and surface runoff are in a cycle with the ocean. Wet lowlands represent a minor surface fraction (22% at 40° obliquity) of the planet for H_2=10% (see Fig. 3).

The rain occurs mainly over the ocean (65% of the total rain), and the ocean evaporation is 60% compensated by rain. The snow precipitation over icy highlands is intense but 80% compensated by high sublimation rates. Our climate model differs from the "icy highlands model" (17) since the ocean is stable.

From these results, one can describe a cold and wet climatic regime (see Fig. 3 bottom) with significant glacier return flow from cold highlands back to the ocean and moderate surface runoff near the shoreline.

Comparison to geological evidence

The proposed scenario is in agreement with a long term stability of the ocean, with the paleo-shoreline and tsunami deposits. In addition, this climatic regime is in agreement with independent geological evidence concerning fluvial and glacial processes. Figure 3 plots the major geological features of similar late Hesperian/early Amazonian age.

Contrary to the Noachian epoch, the modest appearance and development of dendritic valleys (rainfall related) during the late Hesperian/early Amazonian has been tied to major changes in climate. Several valleys at 2.9 Ga have been identified in the North of Alba Patera with a substantial temporal peak in the drainage density (36), located in the dichotomy boundary, in agreement with large rainfall predicted by our model (see Fig. 1). In addition a relatively high density network has been located in the South of Hellas basin (37). Along the highland/lowland boundary (northwestern Arabia Terra and in Deuteronilus Mensae regions) some aligned channels are observed displaying streamlined islands of Hesperian age of possible marine (11) or fluvial origin (38). The wet lowlands have been significantly covered by more recent Amazonian processes (including volcanic resurfacing) (38), erasing most of the geological features of this age available at the surface.

Global extensive ice sheets have been proposed in the Southern hemisphere. Some deposits in the region of Malea Planum (Pityusa Patera) are possible remnants of an extensive polar ice sheet emplaced during the Hesperian period (39, 40). In addition, a 3 Ga old polythermal ice sheet should had covered the entire basin of Isidis Planitia with a maximum thickness of 4.9 km (41, 42). Since this basin is right nearby the 0°C isotherm, a glacier could have flowed from the accumulation zone in the highlands down to the ablation zone in Isidis, as mapped by Jöns (43).

Reull Vallis is a 1500 km long U-shaped valley post-dating the Hesperian ridged plains with a long and complex history (44). It has been carved by glacial flow along the channel during a younger resurfacing episode of late Hesperian-early Amazonian age (45). With a length of $\sim$ 3000 km, $\sim$ 500 km width, and a depth of $\sim$ 3 km, Kasei Valles is the largest outflow channel on Mars. Flooding activity occurred mostly at the Hesperian between 3.6 and 3.8 Ga, with continuing activity possible to 2.5 $\pm$ 1 Ga. (46). The morphology of Kasei Valles region is consistent with an origin by ice with a striking analogy to Alaskan glaciers (47) and Antarctic ice streams (48). A glacial interpretation of the Kasei Valles outflow was also proposed to explain the presence of scour features, tunnel valleys and esker forms (49). Ares Vallis is a 1500 km long Hesperian outflow channel displaying multiple catastrophic flooding events. Its floor shows geomorphological evidence of ice-covered flooding (50) and glacial erosion (51) with subsequent thermokarst degradation (52). The presence of thermokarst lakes formed after flooding (52, 53) supports a hypothesis of the thawing of ground ice during the Hesperian (i.e., 3.6–3.0 Ga). In addition, evidence of past glaciations (between 1.4 Ga to 3.5 Ga) was reported within Valles Marineris.

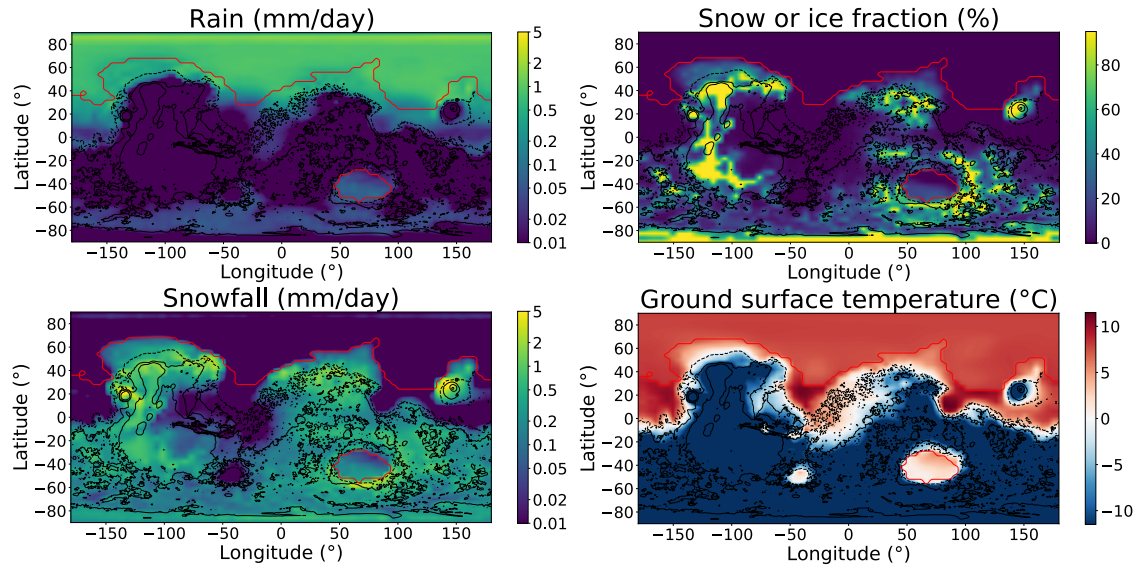

Fig. 1. 3D GCM output at 40° obliquity and H_2=10% for the rain precipitation, snow and ice fraction at the surface, snowfall, sea/ground surface temperature. Black contour lines represent surface elevation level (-2000, 0, 2000 and 8000 meters) and the red contour line is the paleo-shoreline (-3900 meters).

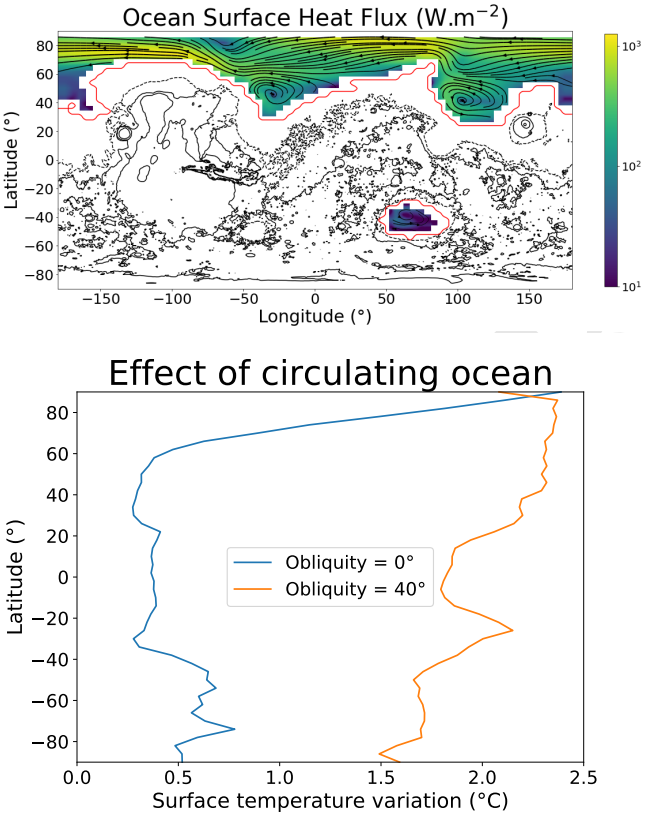

Fig. 2. (top) **REPLACE: with plot of netht_osurf in ANN0310-0319.aijPM01C3.nc (zero obliq) or ANN0310-0319.aijPM03C3.nc (40 obliq) However, please multiple the values by -1 and call it Net Heat Out of Ocean. Igor thinks this is a better term and will give us red at the poles, not blue (the default in panoply). Also use even values on the color bar. This should appease reviewer comment on divergence.** Horizontal surface heat flux transported by the ocean for 40° obliquity and H_2=10%. Streamlines, represented with arrows, show the gyres mainly going poleward and stabilizing the ocean. For a slab ocean model, this flux is null. Black contour lines represent surface elevation level and the red contour line is the paleo-shoreline. (bottom) Latitudinal profile of the temperature increase ($T_{circulating}$-T_{slab}) due to the circulating ocean. In the slab case, the ocean is assumed stratified but non circulating.

Morphological evidence shows that extensive subglacial erosion of the lower parts of Valles Marineris wallslopes, together with sackung deformations by deglaciation of the upper wallslopes occurred (54, 55). Finally, one has to note that the extensive outflow channels are contemporaneous to the ocean. An ocean at the Hesperian is also compatible with the timing of peak outflow channel activities (56, 57). Outflows probably formed by aquifer disruption (58) or glacial erosion (47, 51). More abundant signs of glaciation in the icy highlands may have been prevented by less erosive cold-based glaciers (59) and by post-dating Amazonian processes, such as volcanic events (38).

One also has to remind the arguments that must face the stable ocean scenario. First, the interpretation and location of the paleoshoreline itself is matter of controversy (60, 61). Some studies claimed that the putative shorelines are mutually inconsistent (62) but it mainly concerns Contact 1 (Arabia potential shoreline), not Contact 2 (younger Deuteronilus shoreline) that we actually using in our study. Second, mineralogical data seems inconsistent with an Late Hesperian ocean (63, 64). In particular, mineralogy from impact crater excavated terrains (65) and clays occurence in central peaks (66) are more consistent with a volcanic origin. But a widespread sedimentary rock has been identified in the Northern plains of Mars (67). Last, there is a lack of observed carbonates at the surface, that imply that the ocean was acidic. But acidic ocean seems unfavorable in presence of mafic rocks (68). Scenarios alternative to ocean have been proposed implying lava flows (69) or ice-related processes (56, 70). In addition, crater's ejecta has been proposed as an alternative to tsunami deposits for form the thumbprint terrains (29).

Our results demonstrate that a cold and wet climate could have been stable and coherent with geomorphologic evidence. Using fully coupled atmosphere / dynamic ocean modeling, we show that the ocean's circulation warm regionally the surface by 2.5°C. In these conditions, ocean is stable even for a global mean planetary temperature below 0°C. This Martian climate is similar to the one on the Earth with an active water cycle at the same age of the early stage of Life's appearance. Future work should encompass careful analysis of this stability domain

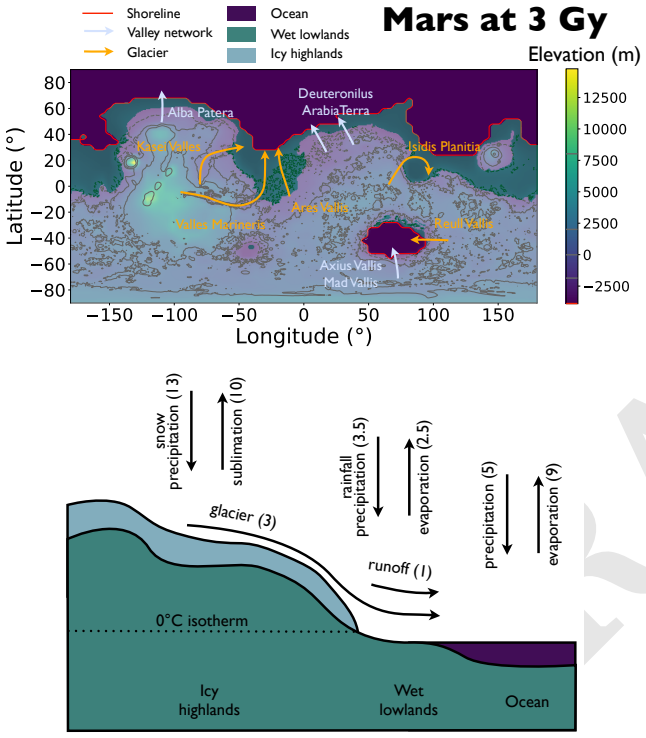

Fig. 3. Proposed scenario of cold and wet climate at the Hesperian age (3 Ga). (top) Map of the climatic zones at 40° obliquity: ocean, wet lowlands and icy highlands, separated respectively by -3900 m and the 0°C isotherm (-1990 m). The topography is modern topography without the North Polar Layered Deposits. Geological evidence of past glaciers with possible paths indicating return flow to the oceans are highlighted. Geological evidence of high drainage density valley networks 3 Ga is rare but noted above. (bottom) Simplified scheme of the hydrological cycle using box modeling. Fluxes in parenthesis have units of 10^{15} kg.y^{-1}.

and its application to the past Martian climate, especially in the Noachian epoch. In addition, we hope that this work will stimulate more precise ice sheet simulations on Mars at global scale, in comparison with detailed photo-geomorphological studies. Further in situ analysis of the ocean boundary, for instance by the Zhurong rover, should confirm the shoreline and tsunami deposits interpretation.

Data Archival. Model runs output will be available here:https://portal.nccs.nasa.gov/GISS_modelE/ROCKE-3D/publication-supplements/

Materials and Methods

3D-GCM. The 3-D General Circulation Model (3D-GCM) simulations performed herein utilize ROCKE-3D (23), which is based upon a parent Earth Climate Model known as ModelE2 (24). ModelE2 has been used for the Coupled Model Intercomparison Project Phase 5 (CMIP5). ROCKE-3D has a number of extensions in areas relative to non-Earth terrestrial worlds (23). In particular ROCKE-3D utilizes a separate and highly flexible radiative transfer scheme known as SOCRATES (71, 72) that allows for non-Earth atmospheric gas constituents and abundances which are outside the capabilities of the native ModelE2 scheme. ROCKE-3D also extends the ModelE2 calendaring system and allows for worlds with different rotational and orbital parameters. In this project we use $4° \times 5°$ horizontal resolution for all components. The atmosphere has 40 layers with upper boundary at 10^{-4} of the surface pressure and the ocean has 13 layers. The major components exchange data at 1850 s time step, though they use shorter time steps internally. We assume the solar luminosity to be $\sim 79\%$ (25) of its current value (1360.67 W m^{-2}) following (73), hence at 3 Ga, the flux at Mars was set to 452.8 W m^{-2}. For this work we rely upon CO_2+H_2 CIA tables from (33). Although recent work (74) has demonstrated the possibility that (33) may overestimate the warming provided in their CO2+H2 CIA calculations (confirmed by (75)). At the same time the ROCKE-3D SOCRATES CO_2 absorption is underestimated and they tend to cancel each other out in experiments conducted in (76).

H_2 provides a powerful greenhouse component in combination with CO_2 as a background gas, but other gas combinations involving CH_4 or H_2S may have an equivalent radiative effect even if the motivation for their use is lacking. Recent measurements of collision induced absorption of CO_1 and CH_4 shows that this possibility is not favored (74). We run simulations with 10% and 20% H_2 in a CO_2 dominated atmosphere at 1 bar surface pressure to simulate the climate at 3 Ga, as in (15). We run simulations with 0°, 20°, 40°, 60° obliquity, since this orbital parameter can have large excursions from the mean value in the past (77, 78).

Short description about cloud modeling (radiatively active/passive, H2O, CO2 ?, precipitation, snow/ice fraction)

The surface radiative properties are described in (79). The spectral and solar zenith angle dependence of ocean albedo is based on calculations of Fresnel reflection from wave surface distributions as a function of wind velocity (80). The effects of foam on ocean albedo are also included (81). In addition, ROCKE-3D also includes the dependance of the cosine of the zenith angle for snow both on the ocean ice and on the land (82).

OGCM. The ocean model assumes Earth's values of salinity (35 PSU) and included XXX processes (sea ice, salinity change due to fresh water incorporation by surface runoff, precipitation and sea ice). The spatial resolution is XXX vertical and XXX vertical. The time step is XXX. Initialization as liquid.

Topography is assumed to be identical to present time (except the cap that are removed). According to topography analysis, the Late Hesperian stage of the paleoshoreline is coherent with current altitude, i.e.: without correction of the True Polar Wander due to Tharsis (4, 5, 83, 84). The ocean shoreline is set to -3900 meters in all runs. This gives an ocean surface fraction of $\sim$16% which is small in comparison to Earth at $\sim$ 71%. The ocean is also shallower

than the mean depth for Earth. For this reason the time to bring our ancient Mars model ocean and atmosphere into equilibrium is much shorter ($\sim$ 100s of years) than would be the case for an Earth like ocean ($\sim$ 1000s of years). We assume this equilibrium has been reached when the net radiative balance (the difference between incoming and outgoing fluxes) is less than 0.2 W m^{-2}. Model runs typically require 300 martian years to reach equilibrium. All outputs are averaged over 10 Martian years, after radiative equilibrium. All quantities are expressed in Earth year, noted "y". When referring about time before present, we used the Earth year ago, noted "a".

Hydrological cycle. In addition to ocean and atmospheric modeling, the model encompasses a surface scheme to simulate the hydrological cycle, including a surface runoff scheme. It is challenging to couple glaciers in GCM simulations due to their much longer time-scales ($\sim 10^{4-5}$ years) versus the typical timescales modeled in 3-D GCM simulations ($\sim 10^{3}$). In CMIP studies ice sheets are normally calculated off-line and incorporated into GCM simulations at different epochs (85). Here we propose a first order simulation : when snow accumulation reaches 1.9 m H_2O equivalent ($\sim$ 6.5m snow), the extra-water ice content is instantaneously moved back to the ocean. This strategy has been used to model Earth climate, for instance the last glacial maximum on Earth, 21,000 years ago (86). The threshold at 1.9 meter is artificial but various test have demonstrated that the final results do not depend on this parameter. This scheme allows one to simulate a static representation of this cold and wet climate. Due to this glacier simulation scheme, the surface ice height is not meaningful. Instead, we focus on the snow/ice fraction inside the grid cell and the mass balance. At the surface temperatures found in our results ($>$ 250K), the ice can easily flow on Mars (87–89)

Box modeling. The complex 3D climate system is summarized by box modeling. We divided the surface into 3 zones : icy highlands, wet lowlands and ocean, delimited respectively by the mean altitude of the 0°C isotherm and -3900 m. For each surface box, but also for the atmosphere and the ocean, we compute the sum of all incoming and outgoing fluxes of water, including snow/rain precipitation, evaporation, surface runoff and simplified glacier return flow (See Sup. Mat. sections 1.2 and 1.3). The porous soil is initiated with fully saturated liquid water that is adjusted according to climatic conditions during the course of the simulation. The timescale for this process to reach equilibrium is possibly much longer ($\sim$ 1000s of years). Since we are not interested in this process, we estimate and remove this source of water flux in our box modeling. The hydrological cycle is in balance by assumption, but there are unaccounted for fluxes at $<= 5\%$ due to incomplete GCM diagnostics, from salinity changes and numerical rounding. Supplementary material presents the mass fluxes of all model runs.

ACKNOWLEDGMENTS. We acknowledge support from the "Institut National des Sciences de l'Univers" (INSU), the "Centre National de la Recherche Scientifique" (CNRS) and "Centre National d'Etudes Spatiales" (CNES) through the "Programme National de Planétologie". M.J.W. was supported by the National Aeronautics and Space Administration (NASA) Astrobiology Program through collaborations arising from his participation in the Nexus for Exoplanet System Science (NExSS) and the NASA Habitable Worlds Program. Resources supporting this work were provided by the NASA High-End Computing (HEC) Program through the NASA Center for Climate Simulation (NCCS) at Goddard Space Flight Center. M. J. W. and A. I. acknowledge support from the GSFC Sellers Exoplanet Environments Collaboration (SEEC), which is funded by the NASA Planetary Science Division's Internal Scientist Funding Model.

1. VR Baker, et al., Ancient oceans, ice sheets and the hydrological cycle on mars. *Nature* **352**, 589–594 (1991).
2. ZI Dickeson, JM Davis, Martian oceans. *Astron. & Geophys.* **61**, 311–317 (2020).
3. TJ Parker, DS Gorsline, RS Saunders, DC Pieri, DM Schneeberger, Coastal geomorphology of the martian northern plains. *J. Geophys. Res.* **98**, 11061 (1993).
4. JW Head, et al., Possible ancient oceans on mars: Evidence from mars orbiter laser altimeter data. *Science* **286**, 2134–2137 (1999).
5. RI Citron, M Manga, DJ Hemingway, Timing of oceans on mars from shoreline deformation. *Nature* **555**, 643–646 (2018).
6. J Mouginot, A Pommerol, P Beck, W Kofman, SM Clifford, Dielectric map of the martian northern hemisphere and the nature of plain filling materials. *Geophys. Res. Lett.* **39**, L02202– (2012).
7. MA Kreslavsky, JW Head, Kilometer-scale roughness of Mars: Results from MOLA data analysis. *J. Geophys. Res.* **105**, 26695–26712 (2000).
8. AA Saberi, Evidence for an ancient sea level on mars. *The Astrophys. J.* **896**, L25 (2020).
9. M Ivanov, G Erkeling, H Hiesinger, H Bernhardt, D Reiss, Topography of the deuteronilus contact on mars: Evidence for an ancient water/mud ocean and long-wavelength topographic readjustments. *Planet. Space Sci.* **144**, 49–70 (2017).
10. S Duran, TJ Coulthard, The kasei valles, mars: a unified record of episodic channel flows and ancient ocean levels. *Sci. Reports* **10** (2020).
11. JAP Rodriguez, et al., Tsunami waves extensively resurfaced the shorelines of an early martian ocean. *Sci. Reports* **6**, 25106– (2016).
12. F Costard, et al., Modeling tsunami propagation and the emplacement of thumbprint terrain in an early mars ocean. *J. Geophys. Res. Planets* **122**, 633–649 (2017).
13. F Costard, et al., The lomonosov crater impact event: A possible mega-tsunami source on mars. *J. Geophys. Res. Planets* **124**, 1840–1851 (2019).
14. RD Wordsworth, The climate of early mars. *Annu. Rev. Earth Planet. Sci.* **44**, 381–408 (2016).
15. M Turbet, F Forget, The paradoxes of the late hesperian mars ocean. *Sci. Reports* **9** (2019).
16. F Forget, et al., 3d modelling of the early martian climate under a denser CO_2 atmosphere: Temperatures and CO_2 ice clouds. *Icarus* **222**, 81 – 99 (2013).
17. R Wordsworth, et al., Global modelling of the early martian climate under a denser CO_2 atmosphere: Water cycle and ice evolution. *Icarus* **222**, 1–19 (2013).
18. M Turbet, F Forget, JW Head, R Wordsworth, 3D modelling of the climatic impact of outflow channel formation events on early mars. *Icarus* **288**, 10–36 (2017).
19. ES Kite, LJ Steele, MA Mischna, MI Richardson, Warm early mars surface enabled by high-altitude water ice clouds. *Proc. Natl. Acad. Sci.* **118** (2021).
20. AG Fairén, A cold and wet mars. *Icarus* **208**, 165–175 (2010).
21. A Kamada, et al., A coupled atmosphere–hydrosphere global climate model of early mars: A 'cool and wet' scenario for the formation of water channels. *Icarus* **338**, 113567 (2020).
22. RM Ramirez, RA Craddock, T Usui, Climate simulations of early mars with estimated precipitation, runoff, and erosion rates. *J. Geophys. Res. (Planets)* **125**, e06160 (2020).
23. MJ Way, et al., Resolving Orbital and Climate Keys of Earth and Extraterrestrial Environments with Dynamics (ROCKE-3D) 1.0: A General Circulation Model for Simulating the Climates of Rocky Planets. *Astrophys. J. Suppl. Ser.* **231**, 12 (2017).
24. GA Schmidt, et al., Configuration and assessment of the giss modele2 contributions to the cmip5 archive. *J. Adv. Model. Earth Syst.* **6**, 141–184 (2014).
25. DO Gough, Solar Interior Structure and Luminosity Variations. *Sol. Phys.* **74**, 21–34 (1981).
26. AD Del Genio, et al., Habitable climate scenarios for proxima centauri b with as dynamic ocean. *Astrobiology* **19**, 1–27 (2019).
27. PR Mahaffy, et al., The imprint of atmospheric evolution in the d/h of hesperian clay minerals on mars. *Science* **347**, 412–414 (2015).
28. EL Scheller, BL Ehlmann, R Hu, DJ Adams, YL Yung, Long-term drying of mars by sequestration of ocean-scale volumes of water in the crust. *Science* **372**, 56–62 (2021).
29. ES Kite, Geologic constraints on early mars climate. *Space Sci. Rev.* **215** (2019).
30. RD Wordsworth, L Kerber, RT Pierrehumbert, F Forget, JW Head, Comparison of "warm and wet" and "cold and icy" scenarios for early mars in a 3-d climate model. *J. Geophys. Res. Planets* **120**, 1201–1219 (2015).
31. RM Ramirez, et al., Warming early mars with CO_2 and H_2. *Nat. Geosci* **7**, 59–63 (2014).
32. N Batalha, SD Domagal-Goldman, R Ramirez, JF Kasting, Testing the early mars H_2–CO_2 greenhouse hypothesis with a 1-d photochemical model. *Icarus* **258**, 337–349 (2015).
33. R Wordsworth, et al., Transient reducing greenhouse warming on early mars. *Geophys. Res. Lett.* **44**, 665–671 (2017).
34. MJ Way, et al., Climates of warm earth-like planets. i. 3d model simulations. *The Astrophys. J. Suppl. Ser.* **239**, 24 (2018).
35. V Radić, R Hock, Glaciers in the earth's hydrological cycle: Assessments of glacier mass and runoff changes on global and regional scales. *Surv. Geophys.* **35**, 813–837 (2013).
36. BM Hynek, M Beach, MRT Hoke, Updated global map of martian valley networks and implications for climate and hydrologic processes. *J. Geophys. Res.* **115** (2010).
37. H Bernhardt, et al., Photogeologic mapping and the geologic history of the hellas basin floor, mars. *Icarus* **264**, 407–442 (2016).
38. KL Tanaka, et al., Geologic map of Mars. *U.S. Geol. Surv. Rep.* **-**, 3292 (2014).
39. JW Head, S Pratt, Extensive hesperian-aged south polar ice sheet on mars: Evidence for massive melting and retreat, and lateral flow and ponding of meltwater. *J. Geophys. Res. Planets* **106**, 12275–12299 (2001).
40. GJ Leonard, KL Tanaka, Geologic Map of the Hellas Region of Mars. *U.S. Geol. Surv. Rep.* **-**, 2694 (2001).
41. O Souček, O Bourgeois, S Pochat, T Guidat, A 3 ga old polythermal ice sheet in isidis planitia, mars: Dynamics and thermal regime inferred from numerical modeling. *Earth Planet. Sci. Lett.* **426**, 176–190 (2015).
42. T Guidat, S Pochat, O Bourgeois, O Souček, Landform assemblage in isidis planitia, mars: Evidence for a 3 ga old polythermal ice sheet. *Earth Planet. Sci. Lett.* **411**, 253–267 (2015).
43. HP Jöns, Large Fossil Mud Lakes or Giant Mud Sheet Floods in Syrtis Major (Isidis Planitia) and Mare Australe, Mars in *Lunar and Planetary Science Conference*, Lunar and Planetary Science Conference. Vol. 18, p. 470 (1987).
44. SC Mest, DA Crown, Geology of the reull vallis region, mars. *Icarus* **153**, 89–110 (2001).
45. VP Kostama, et al., Topographic and morphologic characteristics of reull vallis, mars: Implications for the history of the reull vallis fluvial system. *J. Geophys. Res.* **112** (2007).
46. JC Andrews-Hanna, RJ Phillips, Hydrological modeling of outflow channels and chaos regions on mars. *J. Geophys. Res. Planets* **112** (2007).
47. BK Lucchitta, Ice sculpture in the martian outflow channels. *J. Geophys. Res.* **87**, 9951 (1982).
48. BK Lucchitta, Antarctic ice streams and outflow channels on mars. *Geophys. Res. Lett.* **28**,

403–406 (2001).
49. J Arfstrom, Equatorial ice sheets of mars (2020).
50. D Wallace, C Sagan, Evaporation of ice in planetary atmospheres: Ice-covered rivers on mars. *Icarus* **39**, 385–400 (1979).
51. A Pacifici, G Komatsu, M Pondrelli, Geological evolution of ares vallis on mars: Formation by multiple events of catastrophic flooding, glacial and periglacial processes. *Icarus* **202**, 60–77 (2009).
52. F Costard, V Baker, Thermokarst landforms and processes in ares vallis, mars. *Geomorphology* **37**, 289–301 (2001).
53. N Warner, S Gupta, JR Kim, SY Lin, JP Muller, Hesperian equatorial thermokarst lakes in ares vallis as evidence for transient warm conditions on mars. *Geology* **38**, 71–74 (2010).
54. D Mège, O Bourgeois, Equatorial glaciations on mars revealed by gravitational collapse of valles marineris wallslopes. *Earth Planet. Sci. Lett.* **310**, 182–191 (2011).
55. M Gourronc, et al., One million cubic kilometers of fossil ice in valles marineris: Relicts of a 3.5gy old glacial landsystem along the martian equator. *Geomorphology* **204**, 235–255 (2014).
56. SM Clifford, TJ Parker, The evolution of the martian hydrosphere: Implications for the fate of a primordial ocean and the current state of the northern plains. *Icarus* **154**, 40–79 (2001).
57. N Warner, S Gupta, JP Muller, JR Kim, SY Lin, A refined chronology of catastrophic outflow events in ares vallis, mars. *Earth Planet. Sci. Lett.* **288**, 58–69 (2009).
58. MH Carr, Formation of martian flood features by release of water from confined aquifers. *J. Geophys. Res.* **84**, 2995 (1979).
59. JL Fastook, JW Head, DR Marchant, F Forget, JB Madeleine, Early mars climate near the noachian-hesperian boundary: Independent evidence for cold conditions from basal melting of the south polar ice sheet (dorsa argentea formation) and implications for valley network formation. *Icarus* **219**, 25–40 (2012).
60. MH Carr, JW Head, Oceans on Mars: An assessment of the observational evidence and possible fate. *J. Geophys. Res. (Planets)* **108**, 8–1 (2003).
61. SF Sholes, DR Montgomery, DC Catling, Quantitative high-resolution reexamination of a hypothesized ocean shoreline in cydonia mensae on mars. *J. Geophys. Res. Planets* **124**, 316–336 (2019).
62. SF Sholes, ZI Dickeson, DR Montgomery, DC Catling, Where are mars' hypothesized ocean shorelines? large lateral and topographic offsets between different versions of paleoshoreline maps. *J. Geophys. Res. Planets* **126** (2021).
63. JP Bibring, et al., Global mineralogical and aqueous mars history derived from omega/mars express data. *Science* **312**, 400–404 (2006).
64. J Carter, F Poulet, JP Bibring, N Mangold, S Murchie, Hydrous minerals on mars as seen by the crism and omega imaging spectrometers: Updated global view. *J. Geophys. Res. Planets* **118**, 831–858 (2013).
65. L Pan, BL Ehlmann, J Carter, CM Ernst, The stratigraphy and history of mars' northern lowlands through mineralogy of impact craters: A comprehensive survey. *J. Geophys. Res. Planets* **122**, 1824–1854 (2017).
66. VZ Sun, RE Milliken, Ancient and recent clay formation on mars as revealed from a global survey of hydrous minerals in crater central peaks. *J. Geophys. Res. Planets* **120**, 2293–2332 (2015).
67. MR Salvatore, PR Christensen, Evidence for widespread aqueous sedimentation in the northern plains of mars. *Geology* **42**, 423–426 (2014).
68. PB Niles, et al., Geochemistry of carbonates on mars: Implications for climate history and nature of aqueous environments. *Space Sci. Rev.* **174**, 301–328 (2012).
69. JW Head, Northern lowlands of mars: Evidence for widespread volcanic flooding and tectonic deformation in the hesperian period. *J. Geophys. Res.* **107** (2002).
70. BK Lucchitta, Mars and earth: Comparison of cold-climate features. *Icarus* **45**, 264–303 (1981).
71. JM Edwards, A Slingo, Studies with a flexible new radiation code. I: Choosing a configuration for a large-scale model. *Q. J. Royal Meteorol. Soc.* **122**, 689–719 (1996).
72. JM Edwards, Efficient Calculation of Infrared Fluxes and Cooling Rates Using the Two-Stream Equations. *J. Atmospheric Sci.* **53**, 1921–1932 (1996).
73. MW Claire, et al., The evolution of solar flux from 0.1 nm to 160 nm: Quantitative estimates for planetary studies. *The Astrophys. J.* **757**, 95 (2012).
74. M Turbet, C Boulet, T Karman, Measurements and semi-empirical calculations of CO_2 + CH_4 and CO_2+H_2 collision-induced absorption across a wide range of wavelengths and temperatures. application for the prediction of early mars surface temperature. *Icarus* **346**, 113762 (2020).
75. PJ Godin, et al., Collision-induced absorption of CH_4-CO_2 and H_2-CO_2 complexes and their effect on the ancient martian atmosphere. *J. Geophys. Res. Planets* **125**, e2019JE006357 (2020) e2019JE006357 2019JE006357.
76. SD Guzewich, et al., 3d simulations of the early martian hydrological cycle mediated by a H_2-CO_2 greenhouse. *Earth Space Sci. Open Arch.* **-**, 47 (2021).
77. J Laskar, et al., Long term evolution and chaotic diffusion of the insolation quantities of Mars. *Icarus* **170**, 343–364 (2004).
78. JC Armstrong, CB Leovy, T Quinn, A 1 Gyr climate model for Mars: new orbital statistics and the importance of seasonally resolved polar processes. *Icarus* **171**, 255–271 (2004).
79. GA Schmidt, et al., Present-day atmospheric simulations using GISS ModelE: Comparison to in situ, satellite, and reanalysis data. *J. Clim.* **19**, 153–192 (2006).
80. C Cox, W Munk, Slopes of the sea surface deduced from photographs of sun glitter. *Bull. Scripps Inst. Oceanogr.* **6**, 401–488 (1956).
81. HR Gordon, MM Jacobs, Albedo of the ocean–atmosphere system: influence of sea foam. *Appl. Opt.* **16**, 2257 (1977).
82. WJ Wiscombe, SG Warren, A model for the spectral albedo of snow. i: Pure snow. *J. Atmospheric Sci.* **37**, 2712–2733 (1980).
83. JT Perron, JX Mitrovica, M Manga, I Matsuyama, MA Richards, Evidence for an ancient martian ocean in the topography of deformed shorelines. *Nature* **447**, 840–843 (2007).
84. S Bouley, et al., Late tharsis formation and implications for early mars. *Nature* **531**, 344–347 (2016).
85. A Abe-Ouchi, et al., Ice-sheet configuration in the cmip5/pmip3 last glacial maximum experiments. *Geosci. Model. Dev.* **8**, 3621–3637 (2015).
86. M Kageyama, et al., The pmip4 contribution to cmip6 – part 4: Scientific objectives and experimental design of the pmip4-cmip6 last glacial maximum experiments and pmip4 sensitivity experiments. *Geosci. Model. Dev.* **10**, 4035–4055 (2017).
87. A Colaprete, BM Jakosky, Ice flow and rock glaciers on mars. *J. Geophys. Res. Planets* **103**, 5897–5909 (1998).
88. BK Lucchitta, Antarctic ice streams and outflow channels on mars. *Geophys. Res. Lett.* **28**, 403–406 (2001).
89. JL Fastook, JW Head, DR Marchant, Formation of lobate debris aprons on mars: Assessment of regional ice sheet collapse and debris-cover armoring. *Icarus* **228**, 54–63 (2014).